Programmable droplet manipulation and wetting with soft magnetic carpets

Ahmet F. Demirörs[a,1], Sümeyye Aykut[a], Sophia Ganzeboom[a], Yuki A. Meier[a], and Erik Poloni[a]

[a]Complex Materials, Department of Materials, ETH Zurich, 8093 Zurich, Switzerland

Edited by Dino Di Carlo, University of California, Los Angeles, CA, and accepted by the Editorial Board October 8, 2021 (received for review June 18, 2021)

The ability to regulate interfacial and wetting properties is highly demanded in anti-icing, anti-biofouling, and medical and energy applications. Recent work on liquid-infused systems achieved switching wetting properties, which allow us to turn between slip and pin states. However, patterning the wetting of surfaces in a dynamic fashion still remains a challenge. In this work, we use programmable wetting to activate and propel droplets over large distances. We achieve this with liquid-infused soft magnetic carpets (SMCs) that consist of pillars that are responsive to external magnetic stimuli. Liquid-infused SMCs, which are sticky for a water droplet, become slippery upon application of a magnetic field. Application of a patterned magnetic field results in a patterned wetting on the SMC. A traveling magnetic field wave translates the patterned wetting on the substrate, which allows droplet manipulation. The droplet speed increases with an increased contact angle and with the droplet size, which offers a potential method to sort and separate droplets with respect to their contact angle or size. Furthermore, programmable control of the droplet allows us to conduct reactions by combining droplets loaded with reagents. Such an ability of conducting small-scale reactions on SMCs has the potential to be used for automated analytical testing, diagnostics, and screening, with a potential to reduce the chemical waste.

liquid-infused surface | droplet manipulation | magnetic fields | soft materials | soft actuators

Controlling surface-wetting properties is of interest in anti-icing (1), anti-biofouling (2–4), marine (5), and environmental (6–8) applications. Liquid-infused surfaces recently received significant attention because of their success in achieving such desired wetting properties (9, 10). Additionally, surfaces with switchable wetting properties are especially sought after because they offer two or more desired states serving different functions. Recent advances demonstrated examples of switchable wetting upon optical (11), acoustic (12, 13), electrical (14, 15), mechanical (16, 17), and magnetic (18–21) stimuli. Among these options, magnetic fields offer the advantage of untethered, simple, and strong actuation. However, these demonstrations usually lack the ability to pattern the wetting of the surface in a dynamic manner and were limited in spatial control. Although previous work has successfully demonstrated a patterned wetting surface, this has only been achieved via the microfabrication of static patterns (22, 23). Furthermore, the ability to reversibly locate and manipulate multiple droplets over large distances has been challenging (10, 24, 25) because of the static nature of the manipulation designs (26, 27). Some of the methods based on magnetic fields suffered from contamination in the used magnetic particles, requiring a purification step after transportation (28, 29). The possibility of water droplet transport on magnetically responsive surfaces has also been demonstrated (30, 31). However, this system could not be easily scaled up, the droplet motion was unidirectional (especially in the board-like structures) and limited to the transport of relatively small (1 to 6 μL) droplets. Here, we suggest that external field stimuli can be used to dynamically pattern the substrate wetting. Moreover, a strategy to locally move this stimulus on the substrate can potentially lead to droplet motion. We explore this strategy by creating "soft magnetic carpets" (SMCs) through a scalable self-assembly procedure that is based on the Rosensweig instability. Recently, we used similar SMCs with no infusion layer to transport solid and liquid cargos (32). In the current work, while the carpets are infused with a liquid, they also contain soft magnetic pillars that align with magnetic fields. By placing a patterned magnetic field underneath the carpet, the alignment response of the pillars induces a wetting pattern of pin and slip states, in which the pillars are straight or bent, respectively. While the straight pillars pin the droplets that are placed on the substrate, the bent ones allow droplets to move. Furthermore, by translating this patterned magnetic field, the effect of a magnetic wave is created, leading to the spatial control of the pinned droplets on the substrate and a method that transports large droplets without having contamination. Next, we showcase that the spatial control of multiple droplets allows us to conduct reactions by transporting and sequentially merging droplets loaded with chemicals and biological specimens. The ability of conducting small-scale reactions on a soft carpet can be potentially used to automatize analytical testing and diagnostics at an increased rate and reduced costs due to the limited use of the ingredients.

Results and Discussion

Two-dimensional arrays of magnetically responsive soft pillars exhibiting permanent magnetization were fabricated by spreading a mixture of NdFeB powder and soft silicone matrix (Ecoflex 00–20) on a substrate (Fig. 1 *A* and *B*; see *Materials and*

Significance

A set of magnetically responsive, soft hairs, which form a soft magnetic carpet, can be infused with a liquid to achieve switchable wetting. Applying a pattern of magnetic field results in a reconfigurable wetting pattern on the soft magnetic carpet. Combining this switchable wetting with a travelling magnetic field wave can allow us to spatially manipulate droplets. The efficiency of the droplet manipulation depends on the size and the contact angle of the droplet, which allows a pathway to sort and separate different droplets. Temporal and spatial control over multiple droplets allows us to conduct droplet reactions, which has a potential to be used for automated analytical testing and screening.

Author contributions: A.F.D. designed research; A.F.D., S.A., S.G., Y.A.M., and E.P. performed research; Y.A.M. and E.P. contributed new reagents/analytic tools; A.F.D., S.A., S.G., Y.A.M., and E.P. analyzed data; and A.F.D. and E.P. wrote the paper.

The authors declare no competing interest.

This article is a PNAS Direct Submission. D.D.C. is a guest editor invited by the Editorial Board.

[1]To whom correspondence may be addressed. Email: ahmet.demiroers@mat.ethz.ch.

This article contains supporting information online at http://www.pnas.org/lookup/suppl/doi:10.1073/pnas.2111291118/-/DCSupplemental.

Published November 9, 2021.

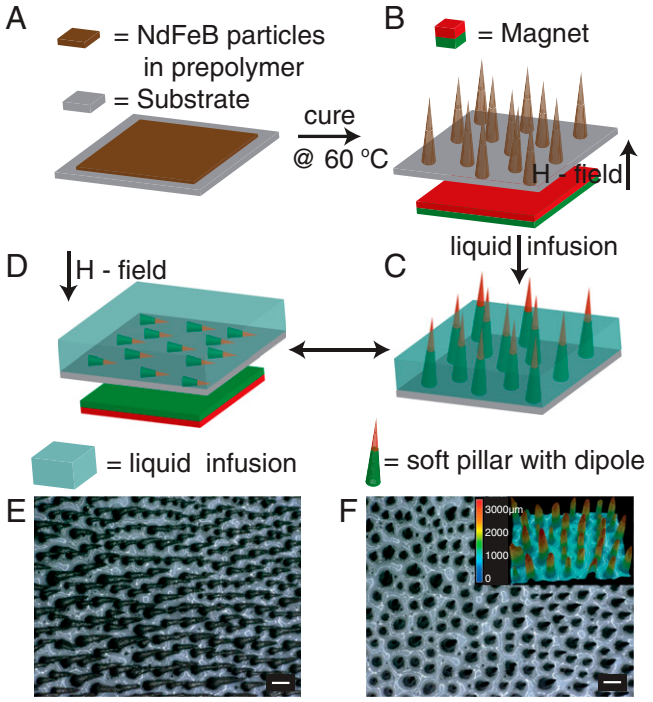

Fig. 1. Fabrication of soft, magnetic carpets with an infusion layer. Schematics of the soft carpet fabrication. (*A*) A prepolymer mixed with NdFeB particles is spread over a substrate. (*B*) Formation of pillar-like structures featuring a magnetic polarization upon exposition to a magnetic field. While being kept at this configuration, the prepolymer is cured at 60 °C, resulting in soft standing pillars with a magnetic dipole determined by the magnet beneath. (*C*) Structures infused with a hydrophobic liquid will exhibit pillars that are straight and reach out of the infusion liquid, thus pinning water droplets on their tips. (*D*) Bending of the pillars upon exposition to a magnetic field opposed to the one in *B* allows for a direct contact of the droplet to the infusion liquid. (*E*) Micrograph of the soft pillars in the slip state, in which they are exposed to a magnetic field of opposite polarization. (*F*) Micrograph of the as-casted soft pillars in the pin state. The inset shows a three-dimensional reconstruction of images taken in reflection mode at different heights of the pillars. (Scale bars, 200 μm.)

Methods and *SI Appendix*, Table S1 for details). During the matrix polymerization, the mixture is exposed to a magnetic field, which induces the formation of pillar-like magnetic particle assemblies embedded in the polymer matrix created by a Rosensweig instability (33). After polymerization, these pillars respond to magnetic fields due to both their magnetization and softness. With magnetic field manipulation, the orientation of the pillars can be deliberately controlled (Fig. 1 *C*–*F*). Here, the soft carpet is infused with a hydrophobic liquid to manipulate the magnetic response of the pillars and change the wetting of the surface. When the pillars are straight and stick out of the infusion liquid, they interact with the droplets by pinning them (Fig. 1*C*). On the contrary, when the micropillars lay flat against the substrate under an external magnetic field, the droplets directly touch the nearly continuous film of lubricant used to infuse the surface (Fig. 1*D*). This allows us to reversibly switch between the two potentially different wetting states via external magnetic manipulation.

In liquid-infused magnetic carpets, the contact angle and the wetting states depend on the applied magnetic field. This allowed us to pattern and dynamically switch the local slip and pin states of the carpets. Because the pillars bend when exposed to magnetic fields with opposite magnetization, their effective height can be tuned. We used their height difference to dynamically change the pin state of the droplets at the surface of an infused liquid: A droplet is pinned when the pillars stick out of the infusion layer but slips when the pillars are magnetically pulled toward the substrate. Because the pillars bend when they are pulled, their height decreases, and the droplet is directly in contact with the infusion liquid. Fig. 2*A* demonstrates and describes the pin and slip states of the system, which could be dynamically switched upon exposition to magnetic fields. To prove the switchability of the surface wetting, we have infused the soft carpet with silicon oil and tilted the surface by 30°. A 30-μL droplet was initially pinned on the carpet, see Fig. 2*B*. The presence of a magnetic field triggered the droplet motion by switching the system to the slip state. The snapshots in Fig. 2*B* show the switching of the slip and pin states with a magnetic field, which determines the motion of the droplet (see also Movie S1). Note here that the driving force for the droplet motion is the gravitational force, while the magnetic field is only responsible for switching the wetting states. The droplet starts to slide when the external body force is larger than the pinning force that holds the droplet on the surface. The pinning force for a droplet on the liquid-infused surface is given by the formula $F_{pin} = \rho V_{drop} g \sin\alpha_{max}$, where ρ and V_{drop} are the density and volume of the droplet, α_{max} is the maximum angle of the droplet staying pinned, and g is the gravitational acceleration (34). The maximum angle of the pinned droplet, α_{max}, has the following relation to the lubricant–droplet contact angle, θ_{ld}, and to the areal fraction of the soft pillars over the whole lubricated surface, ϕ: $\cos\alpha_{max} = \phi\cos\theta_{ld} + (1-\phi)$. Here, θ_{ld} is the contact angle between the silicon oil and the water droplet. On the SMCs, the typical values for the fraction of solid surface, ϕ, lie in the range 0.26 to 0.35 when no magnetic field is applied. However, upon magnetic field manipulation, the fraction of solid surface can be tuned. By decreasing ϕ with the aid of magnetic fields, we can obtain slipping droplets. This is possible because, at low ϕ values, F_{pin} and α_{max} also decrease (e.g., $\alpha_{max} = 9°$ for $\phi = 0.01$). When no magnetic field is applied, $\alpha_{max} = 53°$ at $\phi = 0.3$, which agrees with our experiments. Finally, the droplet-pinning force F_{pin} is 157 μN for a 20-μL droplet at $\phi = 0.3$. This force is also in the proximity of silicone rubber–water adhesion forces (35).

This switch of the surface wetting can be locally performed by using an array of magnets arranged side by side with alternating polarization directions. When such a magnet array is placed under the liquid-infused layer, the surface is patterned with pin and slip states. As shown in Fig. 2*C*, a droplet does not move when placed on a pin area of a carpet tilted by 30° and slips when placed on a slip area. The pattern on the surface can be changed by shifting the magnet array with respect to the substrate. This switches the slip and pin states on the carpet, immediately making the slipping droplet to stop and the pinned one to slip. Snapshots of the carpet in Fig. 2 *C*, *Bottom* demonstrate this dynamic wetting exchange, see also Movie S2. We have characterized the influence of the magnetic field on the contact angle of the droplets to the surface. We found that the contact angle increases with the magnetic field and reaches 120°, which is close to the angle between silicon oil and water (Fig. 2*D*). The velocity of droplets slipping on a tilted substrate increased as the tilt angle was increased from 20 to 50° (Fig. 2*E*). An increase of droplet speed with the tilt angle has been modeled before (36). Here, we also observe an increase in the droplet velocity with tilt angle increase, in agreement with previous report.

We also varied the viscosity of the silicon oil to determine its effect on the velocity of the droplet on tilted substrates. We observed a variation from 7 to 22° in the angle at which the droplet started slipping by changing the viscosity of the silicon oil from 1 to 30,000 cSt (Fig. 2*F*). The dependence of the droplet velocity on the silicon oil viscosity indicates that the water droplet is in the cloaking regime [i.e., the oil spreads over and

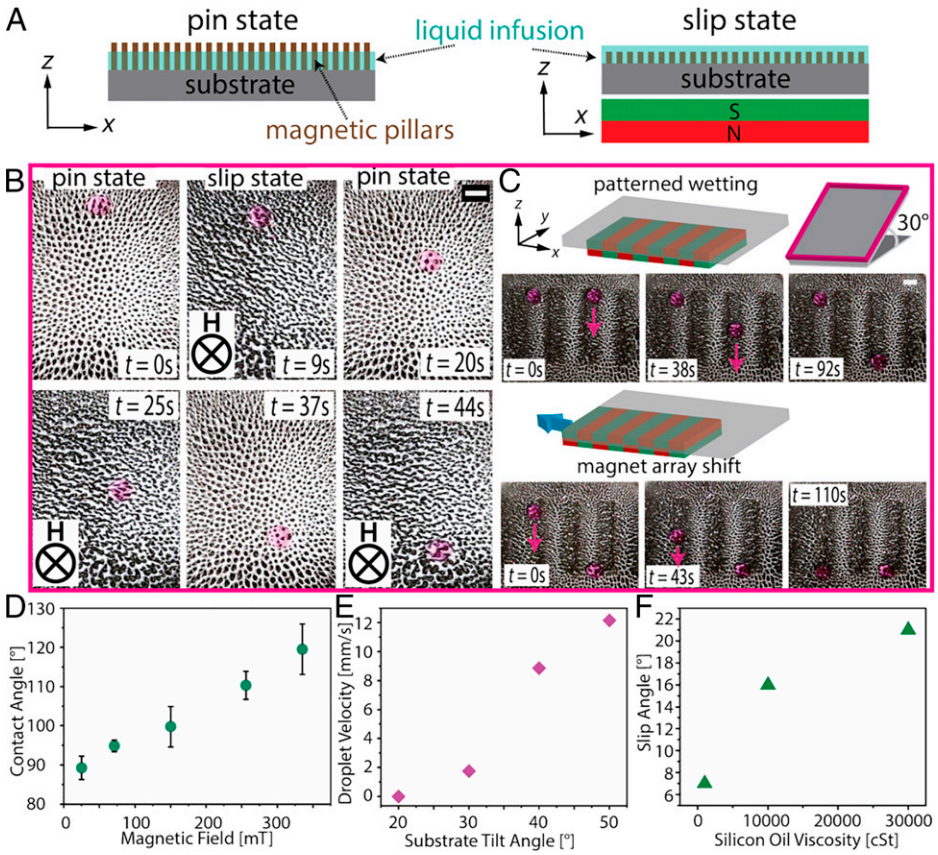

Fig. 2. Switchable and dynamically patternable wetting of the surface via lubricant infusion. (*A*) A sketch depicting the wetting states of the liquid-infused, magnetic carpet without and with a magnetic field of opposite polarization. N and S stand for the north and south pole of the magnet, respectively. (*B*) Time lapse of a 30-μL droplet on a silicon oil-infused carpet. Because the carpet is tilted, the droplet slips when the magnetic field is on and stays pinned when it is off. (*C*) The wetting properties at the surface can be patterned by placing the carpet on a magnet array with alternating field polarizations. Time lapse shows that droplets slip or stay pinned depending on the local wetting of a carpet tilted by 30°. The magnet array can be shifted with respect to the carpet to switch the slip and pin states. (*D*) Contact angle of a droplet on an infused surface as a function of the external magnetic field. (*E*) Velocity of a 30-μL droplet as a function of the tilt angle of the substrate with a silicon oil viscosity of 10,000 cSt. (*F*) Dependence of the minimal slip angle on the viscosity of the silicon oil. (Scale bars, 5 mm.)

"cloaks" the droplet (37)]. This is important because, as a result of the cloaking, the oil interacts with the liquid, causing the droplet slip speed to exhibit a dependence on the oil viscosity. The criterion for cloaking is given by the spreading coefficient, $S_{ow(a)} = \gamma_{wa} - \gamma_{wo} - \gamma_{oa}$, where γ is the interfacial tension between the two phases designated by subscripts *w* (water), *o* (oil), and *a* (air). When $S_{ow(a)} > 0$, the oil will cloak the water droplet, whereas $S_{ow(a)} < 0$ implies otherwise (37). The fact that $S_{ow(a)} \sim 6\,mN/m$ for the silicone oil system agrees with the observed behavior, see *SI Appendix*, Table S2 for details. Up until here, the mobility of the droplet originates from the gravitational and the tilted substrate. However, our soft, responsive substrates may allow for droplet manipulation by a coordinated motion of the soft pillars, enabling capabilities for droplet transfer and manipulation.

The ability to pattern the pin and slip states on the infused soft carpet allows for droplet transportation when the pattern is moved. This motion is achieved by the use of a traveling magnetic field wave. When the magnetic field is translated, the pinning areas are translated with it, which changes the angles of the pinning pillars with respect to the substrate. This change of configuration triggers the repositioning of the droplets pinned at the edge of a pinning area. Additionally, an infusion layer that does not cloak the water droplet may allow for more freedom in the droplet manipulation. To this end, we performed experiments using mineral oil with a negative spreading coefficient $S_{ow(a)} \sim -7\,mN/m$. By exposing a mineral oil–infused soft carpet to a translating magnetic field wave, the droplet moves in a direction opposite to the one of the magnetic field (see *Materials and Methods* and *SI Appendix*, Fig. S1 for magnetic manipulation). The origin of such behavior is described in the sketches and time lapses shown in Fig. 3 *A* and *B*. In these snapshots, while the magnetic field wave is moving to the left, the droplet-pinning pillars are exhibiting a stroke from left to right that pushes the pinned droplet toward the right. Note that effective droplet motion takes place during the backstroke of stretched pillar, which transfers the droplet into a slip region. The droplet stays still at the slip state region, see the middle part of Fig. 3*D*, until the next backstroke wave pins the droplet and transports it further. The shift of the droplet under the effect of a single backstroke is shown in Fig. 3*C* (see also *SI Appendix*, Fig. S2 for the droplet transport mechanism). The stroke yields a droplet displacement of about 2 mm for a 4 mm displacement of the magnetic array (Movie S3). Fig. 3*E* demonstrates the overall droplet motion with the translating magnetic field wave from the top and side views, see also Movies S4 and S5. Similarly, a circular motion of the magnetic field wave can be used to rotate a droplet in a circular path, see Fig. 3 *G* and *H* (Movie S6). We have characterized the droplet motion in relation to the magnetic field translation speed, the droplet size, and the spatial density of the magnetic pillars. For this, we have looked at the droplet transportation of a 30-μL droplet on a SMC (pillar height: 2 mm and

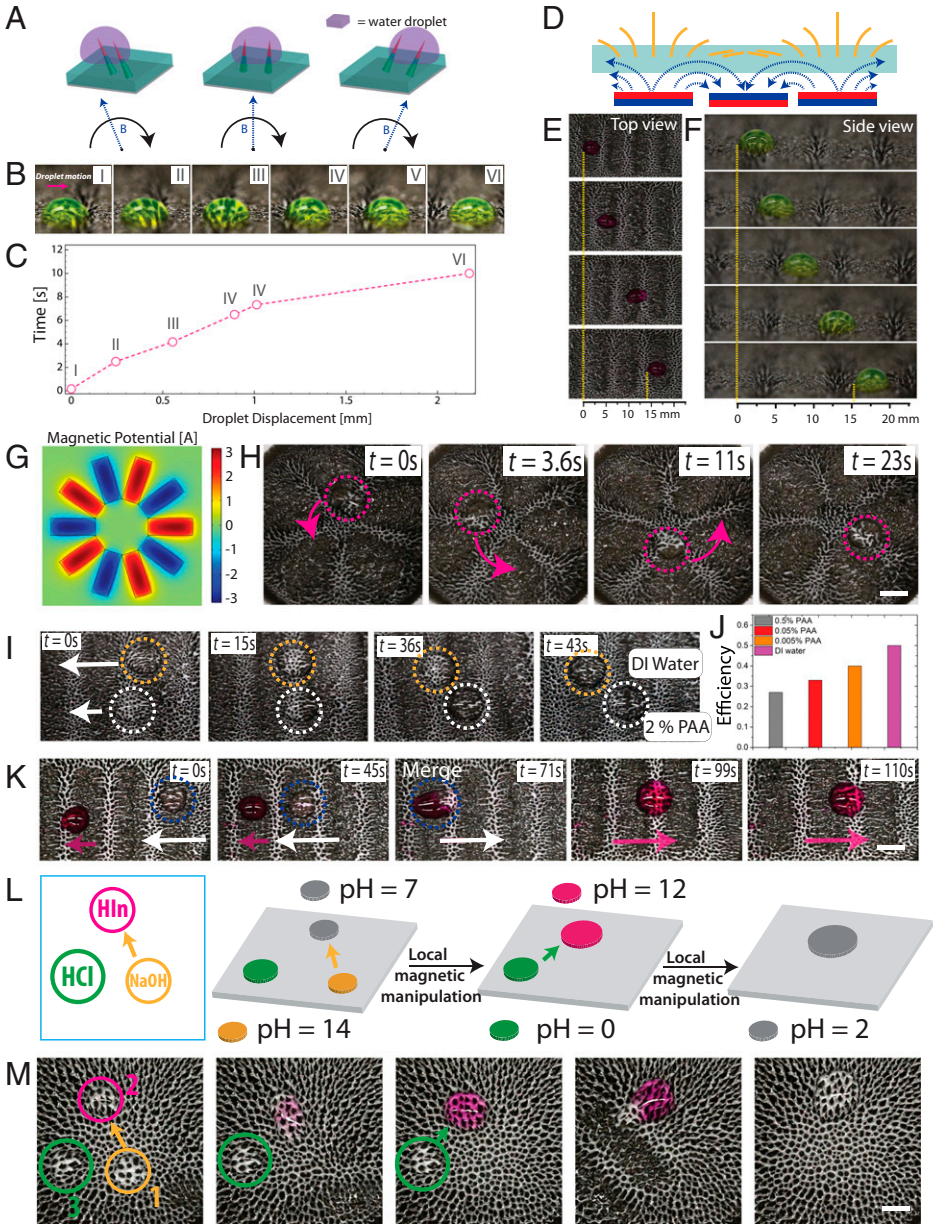

Fig. 3. Droplet transport via relocation of the pinning point. (*A*) Sketches depicting the pinning and the motion of the droplet by the backstroke of the pillar where the droplet pins. Note that the location of the droplet shifts as the pillars wave from left to right. The curved black arrow shows the motion of the pillar tip in time between the frames I through VI in *B* and *C*. (*B*) Snapshots of a single-droplet motion due to the wave movement of the pillars. (*C*) Droplet displacement plotted over time based on the time lapse in *B*. (*D*) A sketch showing the orientation of the pillars exposed to a magnet array. Time lapse of 40-μL droplets moving with a magnetic field wave on a soft carpet: top (*E*) and side views (*F*). The standing pillars that pin the droplet are clearly visible in *F*. (*G*) Magnetic potential of a set of magnets arranged in a rotor shape, which was used for the circular motion of a droplet. (*H*) Time lapse evidencing the droplet motion achieved with rotation of the rotor-shaped magnet shown in *G* set underneath the soft carpet. (*I*) Time lapse of two competing droplets under the influence of the same magnetic field. The deionized (DI) water droplet has a higher-contact angle and moves faster than the 2% PAA droplet. (*J*) Efficiency of the water droplet motion with respect to the translated magnetic field for different PAA surfactant concentrations. The efficiency is taken as the droplet displacement with respect to the displacement of the traveling magnetic field and varies from 0 to 1. (*K*) Time lapse of two droplets that are manipulated to merge and are driven to an opposite direction afterward. The slow pink droplet is merged with a faster water droplet. The PAA droplet is labeled with a rhodamine dye. (*L*) Sketch demonstrating droplet reactions. A neutral droplet carrying a pH indicator (phenolphthalein, HIn) is first merged with a high-pH droplet, changing the color of the neutral droplet to pink because of a pH increase. Next, a low-pH droplet is added to the system, decreasing the pH to an acidic one and yielding a transparent droplet. (*M*) Time lapse of the millifluidic reaction experiment described in *L*, in which the three droplets on the soft carpet are sequentially brought together. The neutral droplet becomes pink and then transparent again. (Scale bars, 5 mm.)

distance between pillars: 1.1 mm) infused with mineral oil at varying magnetic field translation speeds. Although the droplet speed increases with increasing magnetic field translation speed, the efficiency of droplet transport is higher at lower–magnetic field translation speeds. In other words, droplet transport efficiency decreases as the magnetic field translation speed increases (*SI Appendix*, Fig. S3). Furthermore, we have evaluated the lowest limit of the droplet volume that can be transported by using a soft carpet with a higher density of pillars. This soft carpet had a shorter pillar height of 1 mm and an average distance

between pillars of 0.6 mm. Shorter and denser pillars enabled the transport of droplets as small as 2 μL (*SI Appendix*, Fig. S3 *B* and *C*). However, transportation of 5 μL or smaller droplets on a soft carpet with lower density and taller pillars (pillar height 2 mm and distance between pillars 1.1 mm) was not possible, see *SI Appendix*, Fig. S3 *D* and *E*. This suggests that, for an effective droplet transfer, the interpillar distance should be ideally smaller than the size of the droplets. Finally, we noticed that different droplet sizes have different transport efficiencies on the same carpet. Our analyses showed that the efficiency of droplet transportation increased with increasing droplet size, see *SI Appendix*, Fig. S3 *B*, *C*, and *F*. We believe that this ability can potentially be used for size-selective droplet sorting.

In our experiments, we have also observed that the translational speed of the droplet depends on the contact angle of the droplet with the soft carpet surface. To demonstrate this, we have made a set of translation experiments with $1 \times 10^{-3} - 2$ weight percent (wt%) PAA in a water droplet. We found that with increasing surfactant concentration (thus with a decreasing contact angle) the speed and the efficiency of the droplet motion decreased (Fig. 3 *I* and *J* and Movie S7). Here, we define the efficiency as the ratio of the output motion (motion of the droplet) to the input motion, related to the magnetic field wave. In practice, we measure the displacement of the droplet and divide it to the displacement of the magnetic field. This change in the speed of the droplet can be used as a means to sort or merge droplets. In Fig. 3*K*, we have used this velocity change to displace two droplets at different speeds and intentionally merge them for achieving a controlled mixing experiment (Movie S8). It is likely that this speed difference is due to a simple geometric argument, which is the contact area of the droplet to the substrate. The contact area of a droplet increases with a decreasing contact angle. Therefore, the interface energy needed to move the droplet is expected to increase with a decreasing contact angle.

In addition to speed control via contact angle adjustment, local magnetic manipulations can be used to spatially control multiple droplets on the substrate. The ability to control droplet displacements and their merging allows us to use these droplets as cargo carriers to achieve controlled reactions at a droplet scale. To demonstrate the capability of using the droplets as reaction vessels, we have designed droplet-merging experiments carrying different chemistries. In the experiments shown in Fig. 3 *L* and *M*, two transparent 50-μL water droplets became pink when merged. The first droplet had a pH of ∼14 and was composed of 0.5 M NaOH, whereas the second one carried 0.5% phenolphthalein at pH = 7. Phenolphthalein is a pH indicator and changes color when the pH is in the range of 8.2 to 10. It is colorless at acidic pH below 8.2 and becomes pink above a pH 10. By merging these first two droplets, the pH value increased to ∼12, and the phenolphthalein became pink. Subsequentially, the merged droplet was brought together with a third one, carrying 70 μL 1 M HCl (pH = 0), which made the pink droplet transparent again. The first coloration change was due to the high pH, which made the phenolphthalein pink. The third droplet brought the pH back to an acidic value (pH < 7), reverting the droplet color to transparent (Movie S9). The ability to independently relocate multiple droplets allows us to design a vast variety of experiments that can yield a magnetically driven, millifluidic platform with potential applications in laboratory tests and in the pharmacy industry.

An alternative to the hydrophobic oil used in the liquid infusion of the soft carpets is to add a ferrofluid to the oil. This infusion has the potential to allow for more complex droplet manipulation scenarios, as the ferrofluid will interact with the magnetic field and may provide another control parameter. Liquid infusion of the soft carpets with a ferrofluid layer allows for two types of droplet manipulation, which are defined by the height of the layer. When enough ferrofluid is infused in the soft carpet (i.e., when the thickness of the infusion layer is about the pillar height), the magnetic field under the carpet induces a dynamic liquid topography. This topography follows the fingerprints of the magnetic flux density generated by the magnets under the substrate and has round edges due to surface tension and gravitational forces (Fig. 4*A*). Fig. 4*B* shows the magnetic scalar potential associated to the magnetic fields shown in Fig. 4*A*. In this configuration, the flux density dictates the spatial distribution of the ferrofluid, whereas the scalar potential demonstrates the polarization of the magnets and their interaction with the pillars. When the infusion layer boundary is at the height of the pillar or beyond, the surface topography of the ferrofluid dominates the droplet manipulation (Fig. 4 *C* and *D* and Movie S10). This topography follows the magnetic field flux, and the curvature of the surface topography traps the droplet at the slip state. Consequently, the motion of the topography allows for the spatial manipulation of the droplet (Fig. 4*D*) (see also *SI Appendix*, Fig. S4). On the other hand, when the boundary of the ferrofluid layer is below the pillar height (i.e., the thickness of the infusion layer is about 0.5 the pillar height), the pillars of the soft carpet interact with the droplet via pin and slip states.

Compared to mineral oil–infiltrated substrates, this configuration exhibits a more efficient droplet transportation (Fig. 4 *E* and *F* and Movie S11). Note here that the direction of the droplet motion is opposite to the translating magnetic field wave. In this study, the transport efficiency is quantified with a scale varying from −1 to 1 and defined as the ratio between the displacements of the droplet and of the magnet array. When both the droplet and the array move one unit length along the same direction, the efficiency is at its maximum 1, which is the case depicted in Fig. 4 *C* and *D*. For a droplet moving in a direction opposite to the magnetic field motion, the efficiency is negative. Particularly, if both the droplet and the magnet array move one unit in opposite directions, the efficiency is −1. The forward and backward motions observed in Fig. 4 *D* and *F* have an efficiency value of 1 and −0.5, respectively. Moreover, the backward motion for a ferrofluid-infused layer is observed to have a higher transport efficiency than the motion in layers infused only with mineral oil, which lies around −0.4. Although both motions have negative efficiencies, a comparison of their absolute values shows that droplets are transported faster if ferrofluid is added to the infusion layer. The lower efficiency obtained for substrates infused only with mineral oil is explained by the inhomogeneity in the pillar heights. When ferrofluid is added to the infusion layer, the layer also becomes magnetic, forming a topography that improves the distinction between the slip and pin states. The ferrofluid infusion of soft carpets offers an alternative mechanism for droplet manipulation.

Ferrofluid infusion with the rotor-shaped magnet assembly was also demonstrated for droplet manipulation (Fig. 4 *G* and *H* and Movie S12). Because of the circular path formed, this manipulation is only possible with an excess of ferrofluid in the infusion layer. Here, the ferrofluid predominantly occupies the locations with high magnetic flux and forms a topography for the droplets to organize at the gravitational minima in a similar fashion as in Fig. 4 *C* and *D*. When the set of magnets is rotated with one or multiple droplets, these droplets follow the rotation of the magnetic field and exhibit a synchronized circular motion over time (Fig. 4*I* and Movie S13).

Conclusion

By applying external magnetic fields to a liquid-infused soft carpet, patterned and switchable wetting states on the surfaces were achieved. Spatiotemporal control of these wetting states allowed

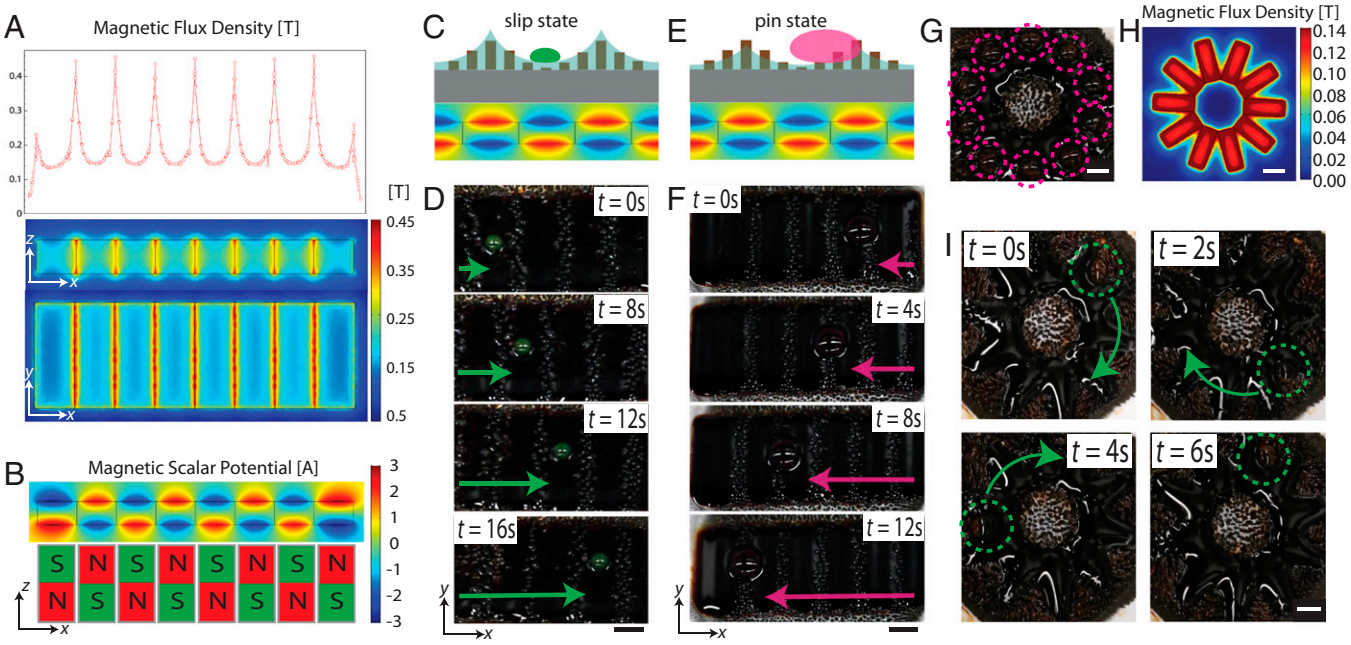

Fig. 4. Droplet transport with a ferrofluid liquid infusion. (*A*) Magnetic flux density over an array of rod-shaped magnets computed with finite element analysis. This magnetic flux density generates the surface topography formed by the ferrofluid infused on the soft carpet. The planes *xz* and *xy* indicate the side and top views, respectively. (*B*) Finite element analysis of the magnetic scalar potential formed on top of a magnet array. The polarization direction (N/S depicts the north and south pole of the magnet, respectively) along the *z*-axis of each magnet in the array is indicated in the sketch. (*C*) Schematics depicting the case of excess ferrofluid in the layer used to infuse the soft carpet. Here, the system stays at the slip state, as the pillar edges are constantly covered by the infusion layer. (*D*) The motion of the surface topography with a moving magnetic wave carries the 20-μL droplet along the same direction of the wave motion. Snapshots show the droplet transport at the slip state over time. (*E*) A sketch depicting the case of a soft carpet infused with a layer poor in ferrofluid. Here, the surface exhibits both pin and slip states. Droplets pin quickly, and the strokes of these pinning pillars drive the droplet motion, similar to the motion mechanism in Fig. 3. (*F*) The strokes of the pinning pillars push the 60-μL droplet in an opposite direction to the moving magnetic field wave. Snapshots show the droplet transport at the pin state over time. (*G*) A rotor-shaped magnet array manipulates ten 50-μL droplets with a ferrofluid infusion. Magnetic flux density of the rotor-shaped magnet array placed under the infused substrate (*H*) and time lapse of a 50-μL water droplet being manipulated on a circular path (*I*). (Scale bars, 5 mm.)

us to design surface forces and manipulate nonmagnetic droplets over the soft pillars infused with a liquid. The infusion of a repellent liquid allows for droplet manipulation without contaminating its content. This enables the use of droplets as small containers to deliver chemical cargo and to combine two distinct chemicals for a reaction or a synthesis. We showcased this capability by merging droplets for specific chemical reactions that demonstrated visual modifications as a result of changing pH values. Furthermore, several control parameters to tune the droplet velocity on the substrate were identified, such as the contact angle, the surfactant concentration, and the use of a ferrofluid infusion layer. We believe that the programmable spatiotemporal control of droplets on a substrate offers the potential for an automated bioanalytical and chemical testing platform, in which small droplets act as tiny test tubes and significantly reduce the amount of sample used per test.

Materials and Methods

Fabrication of the Soft Carpet. To fabricate our soft, magnetic pillars, we modified the method of refs. 38 and 39 by using hard ferromagnetic particles instead of the soft ferromagnetic particles. First, we prepared a mixture of Ecoflex 00–20 (a Platinum Silicone rubber compound, Smooth-on Inc.), hexane (Sigma-Aldrich, ACS reagent), and magnetic neodymium iron boron particles (NdFeB, Magnequench MQFP-B + D50 = ∼25 μm, 10215–088, Lot No. F00492) with a weight ratio of 4:1:x, with x being the NdFeB particle mass. In a typical experiment, we added 4 g Ecoflex, 1 g hexane, and 3.6 g NdFeB powder (47 wt%). Next, this mixture was homogenized in a Thinky mixer (ARE-250) for 3 min at 2,000 rpm. In a typical experiment, 1 g of this mixture was poured into a Teflon Petri dish (3 × 3 cm and 0.25 mm thickness) and spread evenly by moving a permanent magnet (NdFeB, http://www.supermagnete.ch) back and forth underneath close to the teflon dish. Typically, the magnet had a dimension of 5 × 5 × 2 cm and a strength of 0.4 T. We could make different lengths and shapes of pillars by varying the strength of the magnet and the amount of mixture used. Once pillars had formed, we increased the spacing between the magnet and the Petri dish by 0.5 cm and moved this to an oven to be cured for 20 min at 60 °C, which solidified the Ecoflex 00–20. Mechanical properties of the SMC are given in *SI Appendix*, Table S3. A key requirement to obtain a homogeneous SMC is to evenly spread the mixture before applying the magnetic field, which induces the Rosensweig instability. By doing so, we were able to reproducibly obtain evenly sized pillars with a length polydispersity lower than 5%.

The Magnetic Manipulation of SMCs. The magnetic manipulation of the SMCs was achieved by attaching a magnetic track directly to an electric motor or by using a motorized stage to move the magnetic track (see also *SI Appendix*, Fig. S1). The pillar manipulation performed with our array of permanent magnets may, in principle, also be achieved using electromagnets that can generate similarly complex patterns of magnetic nodes and anti-nodes. To facilitate the use of electromagnets, it is recommended to magnetize the SMCs up to their magnetic saturation level (40). This endows the pillars with a much greater permanent dipole moment so that they can be more readily controlled using external fields generated electrically, which are typically weaker.

Liquid Infusion of Soft Carpets. Liquid infusion was performed by using the following oils: silicon oil with several viscosities (1, 1,000, 10,000, and 30,000 cSt of Sigma-Aldrich) and mineral oil (Sigma-Aldrich). The ferrofluid was added by suspending oil-soluble iron oxide nanoparticles (Ferrotec, EMG 1300 M) in mineral oil with a concentration of 1 mg/mL. A small amount of these suspensions was poured on the soft carpets for a low-infusion level, yielding layers with ∼50% the average pillar height for the scarce case.

Contact Angle Measurements. Contact angle measurements were performed at different magnetic fields by taking a sideview picture of the droplet at contact and measuring the angle with ImageJ image analysis software.

Water Droplet Labeling. To label the water droplets, 30 mg rhodamine isothiocyanate or fluorescein isothiocyanate dye was added to 1 mL glycerol. Small aliquots of the liquid were taken for the experiments.

PAA Water Solutions. For the droplet tests, we prepared PAA (Acros, M.W. 5,000 g/mole) at different concentrations, namely at 0.5, 0.05, and 0.005 wt%. These droplets were placed on the substrates with a micropipette.

Data Availability. All study data are included in the article and/or supporting information.

ACKNOWLEDGMENTS. We are very thankful to Prof. André R. Studart at ETH Zurich for support and discussions. This research was supported by the Swiss National Science Foundation through the National Centre of Competence in Research Bio-Inspired Materials (Grant No. 51NF40_182881).

1. M. J. Kreder, J. Alvarenga, P. Kim, J. Aizenberg, Design of anti-icing surfaces: Smooth, textured or slippery? *Nat. Rev. Mater.* **1**, 15003 (2016).
2. D. C. Leslie *et al.*, A bioinspired omniphobic surface coating on medical devices prevents thrombosis and biofouling. *Nat. Biotechnol.* **32**, 1134–1140 (2014).
3. M. J. Kratochvil *et al.*, Slippery liquid-infused porous surfaces that prevent bacterial surface fouling and inhibit virulence phenotypes in surrounding planktonic cells. *ACS Infect. Dis.* **2**, 509–517 (2016).
4. C. Howell, A. Grinthal, S. Sunny, M. Aizenberg, J. Aizenberg, Designing liquid-infused surfaces for medical applications: A review. *Adv. Mater.* **30**, e1802724 (2018).
5. E. Almeida, T. C. Diamantino, O. de Sousa, Marine paints: The particular case of antifouling paints. *Prog. Org. Coat.* **59**, 2–20 (2007).
6. R. K. Manna, P. B. S. Kumar, R. Adhikari, Colloidal transport by active filaments. *J. Chem. Phys.* **146**, 024901 (2017).
7. E. Ueda, P. A. Levkin, Micropatterning hydrophobic liquid on a porous polymer surface for long-term selective cell-repellency. *Adv. Healthc. Mater.* **2**, 1425–1429 (2013).
8. J. Li *et al.*, Hydrophobic liquid-infused porous polymer surfaces for antibacterial applications. *ACS Appl. Mater. Interfaces* **5**, 6704–6711 (2013).
9. P. Baumli *et al.*, Flow-induced long-term stable slippery surfaces. *Adv. Sci. (Weinh.)* **6**, 1900019 (2019).
10. Q. Sun *et al.*, Surface charge printing for programmed droplet transport. *Nat. Mater.* **18**, 936–941 (2019).
11. K. Ichimura, S. K. Oh, M. Nakagawa, Light-driven motion of liquids on a photoresponsive surface. *Science* **288**, 1624–1626 (2000).
12. D. Foresti, M. Nabavi, M. Klingauf, A. Ferrari, D. Poulikakos, Acoustophoretic contactless transport and handling of matter in air. *Proc. Natl. Acad. Sci. U.S.A.* **110**, 12549–12554 (2013).
13. A. Ozcelik *et al.*, Acoustic tweezers for the life sciences. *Nat. Methods* **15**, 1021–1028 (2018).
14. H. Geng, J. Feng, L. M. Stabryla, S. K. Cho, Dielectrowetting manipulation for digital microfluidics: Creating, transporting, splitting, and merging of droplets. *Lab Chip* **17**, 1060–1068 (2017).
15. J. Li, N. S. Ha, T. Liu, R. M. van Dam, C.-J. Kim, Ionic-surfactant-mediated electrodewetting for digital microfluidics. *Nature* **572**, 507–510 (2019).
16. X. Yao *et al.*, Adaptive fluid-infused porous films with tunable transparency and wettability. *Nat. Mater.* **12**, 529–534 (2013).
17. E. De Jong, Y. Wang, J. M. J. Den Toonder, P. R. Onck, Climbing droplets driven by mechanowetting on transverse waves. *Sci. Adv.* **5**, eaaw0914 (2019).
18. Y. Huang *et al.*, A switchable cross-species liquid repellent surface. *Adv. Mater.* **29**, 1604641 (2017).
19. Y. Cui, D. Li, H. Bai, Bioinspired smart materials for directional liquid transport. *Ind. Eng. Chem. Res.* **56**, 4887–4897 (2017).
20. D. Tian *et al.*, Fast responsive and controllable liquid transport on a magnetic fluid/nanoarray composite interface. *ACS Nano* **10**, 6220–6226 (2016).
21. Y. Zhou, S. Huang, X. Tian, Magnetoresponsive surfaces for manipulation of nonmagnetic liquids: Design and applications. *Adv. Funct. Mater.* **30**, 1906507 (2020).
22. N. Vogel, R. A. Belisle, B. Hatton, T.-S. Wong, J. Aizenberg, Transparency and damage tolerance of patternable omniphobic lubricated surfaces based on inverse colloidal monolayers. *Nat. Commun.* **4**, 2167 (2013).
23. X. Luo *et al.*, Slippery shape memory polymer arrays with switchable isotropy/anisotropy and its application as a reprogrammable platform for controllable droplet motion. *Chem. Eng. J.* **403**, 126356 (2021).
24. C. Yang, Z. Zhang, G. Li, Programmable droplet manipulation by combining a superhydrophobic magnetic film and an electromagnetic pillar array. *Sens. Actuators B Chem.* **262**, 892–901 (2018).
25. A. Li *et al.*, Programmable droplet manipulation by a magnetic-actuated robot. *Sci. Adv.* **6**, eaay5808 (2020).
26. J. Li *et al.*, Oil droplet self-transportation on oleophobic surfaces. *Sci. Adv.* **2**, e1600148 (2016).
27. C. Yu *et al.*, Drop cargo transfer via unidirectional lubricant spreading on peristomemimetic surface. *ACS Nano* **12**, 11307–11315 (2018).
28. Y. Zhang, N.-T. Nguyen, Magnetic digital microfluidics—A review. *Lab Chip* **17**, 994–1008 (2017).
29. M. Latikka, M. Backholm, J. V. I. Timonen, R. H. A. Ras, Wetting of ferrofluids: Phenomena and control. *Curr. Opin. Colloid Interface Sci.* **36**, 118–129 (2018).
30. S. Jiang *et al.*, Three-dimensional multifunctional magnetically responsive liquid manipulator fabricated by femtosecond laser writing and soft transfer. *Nano Lett.* **20**, 7519–7529 (2020).
31. Y. Song *et al.*, Cross-species bioinspired anisotropic surfaces for active droplet transportation driven by unidirectional microcolumn waves. *ACS Appl. Mater. Interfaces* **12**, 42264–42273 (2020).
32. A. F. Demirörs *et al.*, Amphibious transport of fluids and solids by soft magnetic carpets. *Adv. Sci. (Weinh.)* 10.1002/advs.202102510. (2021).
33. R. E. Rosensweig, *Ferrohydrodynamics* (Courier Dover Publications, 1997).
34. M. S. Sadullah, J. R. Panter, H. Kusumaatmaja, Factors controlling the pinning force of liquid droplets on liquid infused surfaces. *Soft Matter* **16**, 8114–8121 (2020).
35. G. Hou *et al.*, Foolproof method for fast and reversible switching of water-droplet adhesion by magnetic gradients. *ACS Appl. Mater. Interfaces* **9**, 23238–23245 (2017).
36. T. Maurer, A. Mebus, U. Janoske, Water Droplet Motion on an Inclining Surface, Paper No. 143, in *Proceedings of the 3rd International Conference of Fluid Flow, Heat and Mass Transfer (FFHMT'16)* (Avestia Publishing, 2016).
37. J. D. Smith *et al.*, Droplet mobility on lubricant-impregnated surfaces. *Soft Matter* **9**, 1772–1780 (2013).
38. H. Lu *et al.*, A bioinspired multilegged soft millirobot that functions in both dry and wet conditions. *Nat. Commun.* **9**, 3944 (2018).
39. J. V. I. Timonen *et al.*, A facile template-free approach to magnetodriven, multifunctional artificial cilia. *ACS Appl. Mater. Interfaces* **2**, 2226–2230 (2010).
40. H. Gu *et al.*, Magnetic cilia carpets with programmable metachronal waves. *Nat. Commun.* **11**, 2637 (2020).